

## Supplementary information

### Electrostatic modulation of thermoelectric transport properties of 2H-MoTe<sub>2</sub>

Tianhui Zhu, Sree Sourav Das, Safoura Nayeb Sadeghi, Farjana Ferdous Tonni, Sergiy Krylyuk, Costel Constantin, Keivan Esfarjani, Albert V. Davydov, and Mona Zebarjadi

#### X-ray diffraction of single crystal bulk MoTe<sub>2</sub>

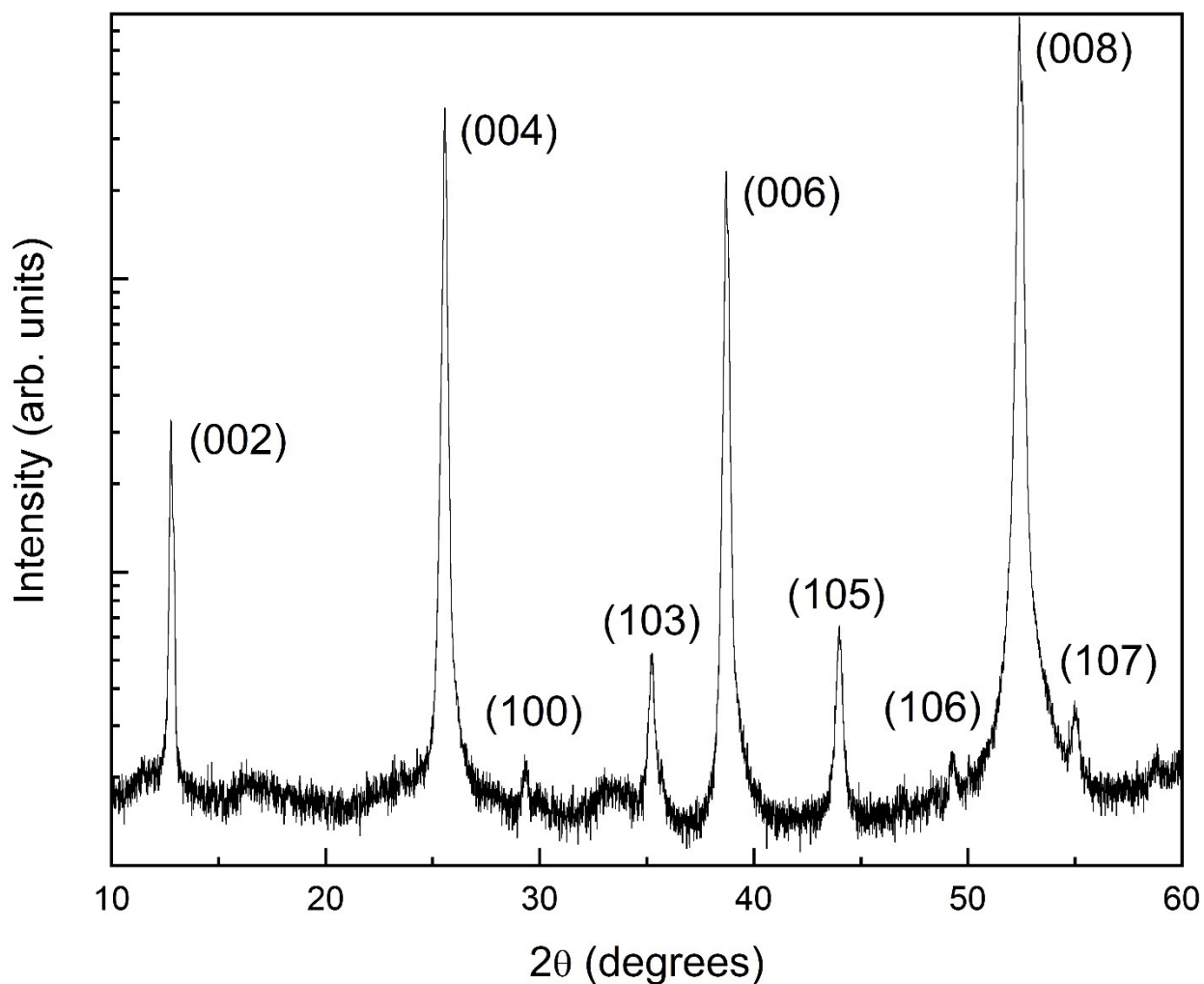


Figure S1 Powder X-ray diffraction pattern of MoTe<sub>2</sub>. The peak positions and *hkl* assignment correspond to the 2H crystal structure (PDF# 72-0117, space group P6<sup>3</sup>/mmc) with the refined lattice parameters *a* = 3.523(1) Å and *c* = 13.981(2) Å.

## Electrical transport of additional device

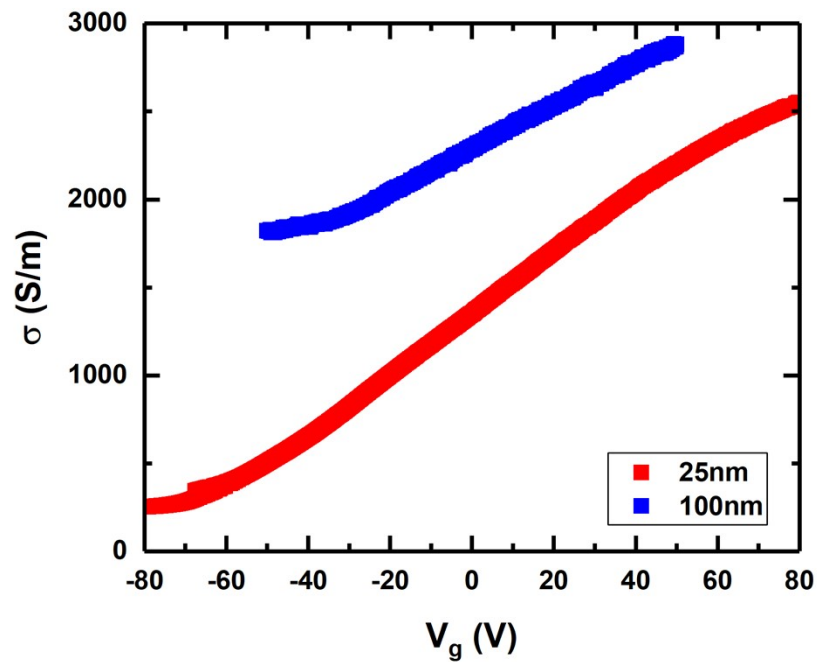


Figure S2 Electrical conductivity versus applied back gate voltage of the 25 nm sample in the main text compared with a second device of 100 nm in thickness.

The electrical conductivity of a second MoTe<sub>2</sub> device of 100 nm in thickness was measured as a function of the back gate bias. Both devices show similar trends with the electrostatic doping and the values are in a similar range.

## Determination of flake thickness using AFM

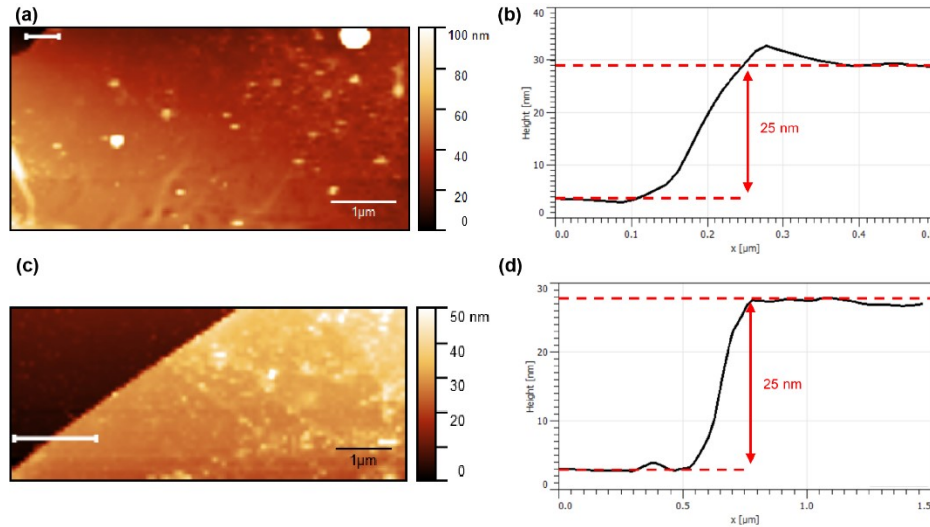


Figure S3 AFM scans and the corresponding step profile for thickness determination. (a) AFM scan and (b) step profile of the 25nm thick sample for electrical transport measurement. (c) AFM scan and (d) step profile of the 25nm thick sample for thermal transport measurement. The uncertainty in thickness is estimated to be about 1nm.

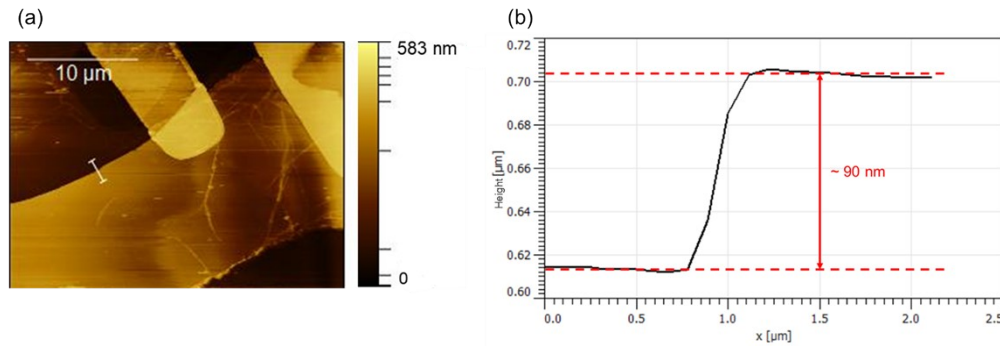


Figure S4 AFM scans and the corresponding step profile for thickness determination. (a) AFM scan and (b) step profile of the 90nm thick sample for thermal transport measurement.

## BoltzTrap calculation details

The Seebeck coefficients and electrical conductivities were calculated using BoltzTraP package<sup>1</sup> with a semi-classical Boltzmann transport method in the constant relaxation time approximation (CRTA)<sup>2</sup>. At a chemical potential of 0.600 eV above the intrinsic fermi level, the Seebeck coefficient is  $-255 \mu\text{V/K}$  and the electrical conductivity is around 2018 S/m with the constant relaxation time ( $\tau$ ) of 0.94 fs. The constant value of relaxation time is obtained using the formula shown below considering the scattering of electron-phonon from PERTURBO and ionized impurity from Brook's Herring Approach.

$$\tau = \frac{\sum \tau(E) \frac{df}{dE}}{\sum \frac{df}{dE}}$$

Constant relaxation time,

where  $\tau(E)$  is the total scattering time including electron-phonon and ionized impurity scattering and the Fermi window used for averaging was  $\mu - 20K_B T$  to  $\mu + 20K_B T$ .

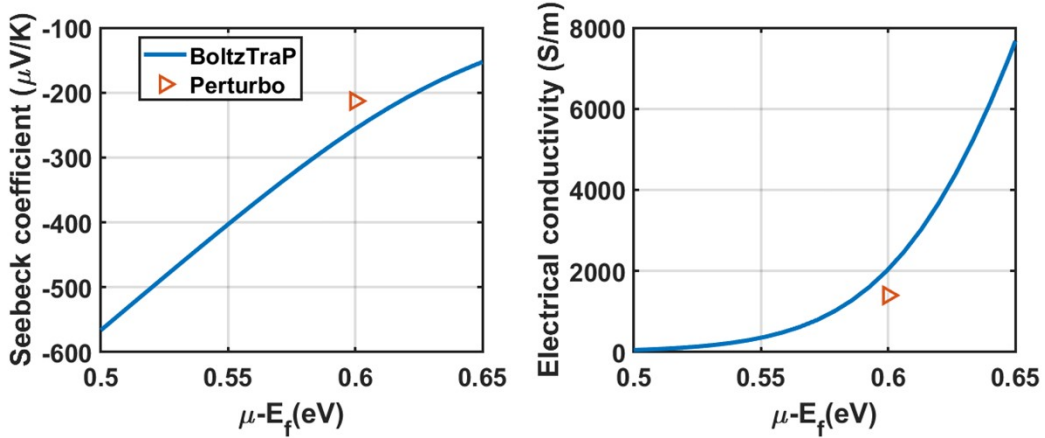


Figure S5: Room temperature Seebeck coefficient and electrical conductivity versus chemical potential for bulk  $\text{MoTe}_2$  with the constant relaxation time  $\tau$  of 0.94 fs.

### Notes on heat diffusion imaging method

Heat diffusion imaging is developed after the heat spreader method<sup>3</sup> where discrete thermal sensors are replaced by a continuous thermal imaging map of temperature. A gold line heater is deposited on top of the supported flake and is pulsed to create Joule heating. The heating results in an exponential temperature decay at the top surface and in the direction perpendicular to the heater. The surface temperature is measured by the thermoreflectance imaging technique, based on the change in the surface reflectivity  $R$ . The relation between  $R$  and  $T$  is

expressed as  $\Delta T = \frac{1}{C_{TR}} \frac{\Delta R}{R}$ , where  $C_{TR}$  is the thermoreflectance coefficient.

Using thermal imaging, we measure  $T(x)$  along many lines, all on the top surface and perpendicular to the heater. We know the temperature should decay exponentially:  $T \propto e^{-\beta x}$ . Hence we use this relation to find  $\beta$  as a fitting parameter and we average over many cycles as well as many lines to minimize our error bar.

$\beta$  is related to the in-plane thermal conductivity,  $k$ , of the sample as  $\beta = \sqrt{h_i / (kd)}$ , where  $h_i$  is the cross-plane thermal conductance of the underlying insulating substrate and  $d$  is the sample thickness. Assuming the same substrate is used, a smaller sample thickness or smaller thermal conductivity means larger  $\beta$  and a faster temperature decay. As the spatial resolution of the

thermoreflectance-based temperature maps is diffraction-limited and is on the order of 100 nm, a shorter decay length gives us fewer data points for the exponential fit and leads to reduced sensitivity and accuracy. When the decay length approaches the diffraction limit, we are not able to extract meaningful data. Previous experiments have demonstrated that the heat spreader principles can be applied to samples down to few or mono-layer limits<sup>4,5</sup>, which means heat diffusion imaging should have enough sensitivity for the thin MoTe<sub>2</sub> flakes of tens of nm in thickness.

## References

- (1) Madsen, G. K. H.; Singh, D. J. BoltzTraP. A Code for Calculating Band-Structure Dependent Quantities. *Comput. Phys. Commun.* **2006**, *175* (1), 67–71. <https://doi.org/10.1016/j.cpc.2006.03.007>.
- (2) Nag, B. R. *Electron Transport in Compound Semiconductors*; Springer Science & Business Media, 2012; Vol. 11.
- (3) Dames, C. MEASURING THE THERMAL CONDUCTIVITY OF THIN FILMS: 3 OMEGA AND RELATED ELECTROTHERMAL METHODS. *Annu. Rev. Heat Transf.* **2013**, *16* (1), 7–49. <https://doi.org/10.1615/AnnualRevHeatTransfer.v16.20>.
- (4) Jang, W.; Chen, Z.; Bao, W.; Lau, C. N.; Dames, C. Thickness-Dependent Thermal Conductivity of Encased Graphene and Ultrathin Graphite. *Nano Lett.* **2010**, *10* (10), 3909–3913. <https://doi.org/10.1021/nl101613u>.
- (5) Zhu, T.; Litwin, P. M.; Rosul, M. G.; Jessup, D.; Akhanda, M. S.; Tonni, F. F.; Krylyuk, S.; Davydov, A. V.; Reinke, P.; McDonnell, S. J.; Zebarjadi, M. Transport Properties of Few-Layer NbSe<sub>2</sub>: From Electronic Structure to Thermoelectric Properties. *Mater. Today Phys.* **2022**, *27*. <https://doi.org/10.1016/j.mtphys.2022.100789>.